ZooKeys

Endoxocrinus (*Diplocrinus*) *kexuei*, a new species of stalked crinoid (Echinodermata, Crinoidea, Isocrinida, Balanocrinidae) from rotten wood in the cold seep area of the Taixinan Basin, South China Sea

Shao'e Sun[1,2,3,4], Zijie Mei[1], Zhongli Sha[1,2,3,4]

1   Department of Marine Organism Taxonomy & Phylogeny, Institute of Oceanology, Chinese Academy of Sciences, Qingdao 266071, China
2   Laboratory for Marine Biology and Biotechnology, Qingdao Marine Science and Technology Center, Qingdao 266237, China
3   Shandong Province Key Laboratory of Experimental Marine Biology, Institute of Oceanology, Chinese Academy of Sciences, Qingdao 266071, China
4   University of Chinese Academy of Sciences, Beijing 100049, China

Corresponding author: Zhongli Sha (shazl@qdio.ac.cn)

Citation: Sun S'e, Mei Z, Sha Z (2025) *Endoxocrinus* (*Diplocrinus*) *kexuei*, a new species of stalked crinoid (Echinodermata, Crinoidea, Isocrinida, Balanocrinidae) from rotten wood in the cold seep area of the Taixinan Basin, South China Sea. ZooKeys 1241: 185–204. https://doi.org/10.3897/zookeys.1241.128991

Abstract

A new species of stalked crinoid, *Endoxocrinus* (*Diplocrinus*) *kexuei* **sp. nov.** belonging to the family Balanocrinidae, is described from cold seeps in the South China Sea. The general appearance of the new species is similar to *E.* (*Diplocrinus*) *alternicirrus*, but can be distinguished from its congener in both morphological characteristics and significant genetic divergences. *Endoxocrinus* (*Diplocrinus*) *kexuei* **sp. nov.** shows cryptosymplexies without marked symmorphy, and an axial canal usually incompletely filled with a lattice needlelike network, preserving an irregular secondary lumen. The new species attribution is well supported by genetic distance based on the mitochondrial *c* oxidase subunit I (*COI*), and molecular phylogenetic analyses based on *COI* and *16S* rRNA. This discovery enhances our understanding of species diversity of *Endoxocrinus* crinoids in the South China Sea.

Key words: Cold seeps, *Endoxocrinus*, new species, South China Sea, stalked crinoids, systematics

Introduction

The order Isocrinida Sieverts-Doreck, 1952 comprises species that are among the most prevalent post-Paleozoic stalked crinoids, found both in the fossil record and among living crinoids (Améziane et al. 2023). The extant Isocrinida diverged into two major lineages during the Middle Triassic, generally recognized as two distinct families: Isocrinidae Gislén, 1924 (including Isocrininae and Metacrininae) and Balanocrinidae Roux, 1981 (including Balanocrininae, Diplocrininae, Isselicrininae, and Proisocrininae) (Améziane et al. 2023). They exhibit a heteromorphic pentaradiate stalk with nodals that carry cirri, and a flexible pinnulate crown typically possessing ten or more arms (David et al. 2006). The subfamily Diplocrininae, which separated from Balanocrininae during the Early Cretaceous, is distinguished by a notable shortening of the brachitaxes, the

widespread replacement of axial synarthries in the arms with synostoses, and the consistent presence of paedomorphic symplexies in the stalk (Roux et al. 2009; Améziane et al. 2023). Diplocrininae is primarily found in the western tropical and northeastern Atlantic, the northern Indian Ocean, and the western and central Pacific, typically inhabiting depths ranging from about 200 to 2000 meters. (David et al. 2006). They grow on slopes and seamounts, thriving on both unconsolidated and rocky substrates (Améziane and Roux 1997; David 1998; David et al. 2006). Two extant genera, *Teliocrinus* Döderlein, 1912 and *Endoxocrinus* A.H. Clark, 1908, are currently attributed to Diplocrininae.

The main characters of the genus *Endoxocrinus* are: (1) IBr2ax, (2) arm branching usually endotomous, (3) B_{r1+2} of each brachitaxis connected by synostosis with small patches of syzygial stereom, and (4) mature symplexies and cryptosymplexies without an interpetaloid groove (David et al. 2006). The genus *Endoxocrinus* is subdivided into two subgenera, *E.* (*Endoxocrinus*) A.H. Clark, 1908 and *E.* (*Diplocrinus*) Döderlein, 1912. The sole species in the subgenus *E.* (*Endoxocrinus*) has more brachitaxis; the number of internodals in each mature noditaxis ranges from 3 to 16; a distal callus at the end of the stalk is rarely present; and the number of cirrals per cirrus varies from 25 to 43, with the mode typically exceeding 30, and the proximal cirri are either perpendicular to the stem or pointing downward (David et al. 2006). *Endoxocrinus* (*Diplocrinus*) spp., usually have two brachials in all brachitaxes; the number of internodals per mature noditaxis is strongly variable; usually with a callus on the distal facet of the distalmost nodal, and with proximal cirri pointing in variable directions (David et al. 2006). The subgenus *E.* (*Endoxocrinus*) is monospecific with *E.* (*Endoxocrinus*) *parrae* (Gervais in Guérin, 1835); whereas *Endoxocrinus* (*Diplocrinus*) includes three species, *E.* (*Diplocrinus*) *alternicirrus* (Carpenter, 1882), *E.* (*Diplocrinus*) *maclearanus* (Thomson, 1878), and *E.* (*Diplocrinus*) *wyvillethomsoni* (Thomson, 1872).

David et al. (2006) conducted a revision of the stalked crinoid species attributed to *Endoxocrinus*, in which ecophenotypic variations have been documented, highlighting the differences between adaptive and phylogenetically indicative traits. David et al. (2006) identified three ecophenotypes of *E.* (*Endoxocrinus*) *parrae* (Gervais in Guérin, 1835) assigned as subspecies: *E.* (*Endoxocrinus*) *parrae parrae* (Gervais in Guérin, 1835), *E.* (*Endoxocrinus*) *parrae prionodes* H. L. Clark, 1941 and *E.* (*Endoxocrinus*) *parrae carolinae* (A. H. Clark, 1934). Similarly, *E.* (*Diplocrinus*) *alternicirrus* includes three subspecies adapted to different habitats: *E.* (*Diplocrinus*) *alternicirrus* (Carpenter, 1882) and *E.* (*Diplocrinus*) *sibogae* (Döderlein, 1907).

Cold seeps are inhabited by a chemosynthetic community that utilizes released reduced compounds, primarily methane and hydrogen sulfide (Kato 2019). Compared to mollusks and arthropods, echinoderms are extremely rare in cold seeps, and paleoecological information of fossil echinoderms in or near cold seep environments is also sporadic (Hunter et al. 2016; Kato 2019; Forel et al. 2024). Since the identification of the first cold seep system in the northern South China Sea in 2004, over 40 active and ancient cold seeps have been found in regions such as the Qiongdongnan Basin, Xisha area, Shenhu area, Dongsha area, and Taixinan Basin (Berndt et al. 2014; Feng et al. 2018; Zhang et al. 2021). Studies on the species diversity of crinoids in the cold seep regions of the South China Sea are underdeveloped. Crinoids are generally not

reported in cold seeps (Kato et al. 2017). Currently, only a few fossil isocrinids have been discovered in cold seep areas worldwide. Hunter et al. (2016) found a new stalked crinoid (*Lakotacrinus brezinai*) from cold methane seeps in the Upper Cretaceous (Campanian) Pierre Shale, South Dakota, United States. Kato (2019) discovered fossil Isocrinina crinoids in the Upper Cretaceous cold seep deposits of the Yezo Group, Hokkaido, Japan. Forel et al. (2024) found some crinoids from the deposits at Sahune, Drôme, south-eastern France Basin, Middle Oxfordian, Late Jurassic.

During our surveys (Institute of Oceanology, Chinese Academy of Sciences) of the deep-sea fauna in the Northwestern Pacific Ocean in 2016, two unusual specimens of *Endoxocrinus* were discovered in the cold seep in the Taixinan Basin, South China Sea. Morphological examination and molecular phylogenetic analysis suggested that these specimens differ from other species of *Endoxocrinus*. Here, we describe them as a new species belonging to the subgenus *Diplocrinus* in the genus *Endoxocrinus*: *Endoxocrinus* (*Diplocrinus*) *kexuei* sp. nov.

Material and methods

Sampling and preservation

We conducted a deep-sea biodiversity survey in the Northwestern Pacific Ocean on 8 September, 2016, where we collected two specimens from a rotten piece of wood in the cold seep area of the Taixinan Basin, South China Sea. The two specimens were collected with a manipulator by the remotely operated submersible (ROV) *FaXian* (Discovery in Chinese) at a depth of 833.7 m, station FX-Dive125 (22°02.58'N, 118°46.83'E). The two specimens were preserved in 70% ethanol and deposited at the Marine Biological Museum of the Chinese Academy of Sciences (MBMCAS), Institute of Oceanology, Chinese Academy of Sciences (IOCAS). Holotype: MBM287584; Paratype: MBM287585.

Morphology observations

Linear architectural characteristics (≥1 mm) of preserved specimens were measured with digital vernier calipers. For the curvilinear structures which were difficult to measure, a ZEISS Axiocam 506 (Carl Zeiss AG, Oberkochen, Germany) microscope camera was used to take photographs, and the Leica LAS Image Analysis software was used to conduct the measurements. Line drawings were completed in Adobe Photoshop 2021 using a graphics tablet. Measurements were rounded to the nearest 0.1 mm. Ossicles of the stalk and arm were dissociated with a 10% aqueous sodium hypochlorite solution until soft tissue was digested. Then the ossicles were rinsed with cold distilled water and dried at room temperature. Scanning electron microscope (SEM) observations were conducted using a Hitachi S-3400N SEM at an accelerating voltage of 5 kV.

The previous revision of pentacrinid stalked crinoids of the genus *Endoxocrinus* (David et al. 2006) and several published keys for different modern stalked crinoid (Roux et al. 2002) were used for the identification of *Endoxocrinus* species. We refer the reader to David et al. (2006) for morphology of *Endoxocrinus* and Roux (1977) for articulations of extant isocrinids. The abbreviations used herein are listed in Table 1.

Table 1. Quantitative morphological characters and the abbreviations of the holotype (MBM287584) and paratype (MBM287585) of *Endoxocrinus* specimens from South China Sea attributed to *E. (Diplocrinus) kexuei* sp. nov. For abbreviations see text. Measurements in mm. *indicate measurements done on the figure instead of the animal. [a] measurement based on remaining stalk length of paratype.

Abbreviations	Diagnostic characters	Holotype	Paratype
dp	proximal diameter of stalk	5	4.4
dd	distal diameter of stalk	4.3	3.7*
sL	stalk length	65	34.97*(17[a])
InN	number of internodals per noditaxis	5	5*
nL	length of noditaxis	7.8	5.9*
InL	internodal length	1.4	0.8*
nL	nodal length	2.5	2.09*
cL	cirrus length	37.1	34.5*
cN	number of cirrals per cirrus	30	—
c_1L	length of first cirral	0.9	—
c_1W	width of first cirral	2.1	—
c_LL	longest cirral length	1.74	—
c_LW	longest cirral width	1.65	—
Arms	number of arms	22	20
bW	basal width	1.7	1.4
bL	basal length	1.1	1.4
rW	radial width	5.1	4.1
rL	radial length	1.8	1.2
p_1L	length of first pinnule	10.8	8.1
p_{1N}	number of pinnulars on first pinnule	11	9
p_1L	first pinnular of first pinnule length	0.9	1
p_1W	width of first pinnular of first pinnule	1.4	1.1

DNA extraction, sequencing and phylogenetic analyses

Both *Endoxocrinus* specimens were prepared for DNA barcoding. All genomic DNA was obtained from pinnules using the E.Z.N.A.® Tissue DNA Kit (Omega-biotek, Inc., Norcross, Georgia, USA) according to the manufacturer's instructions. The DNA was eluted using sterile distilled water and stored at −20 °C. Two mitochondrial markers, cytochrome *c* oxidase subunit I (*COI*) and large ribosomal RNA (16S rRNA), and one nuclear marker, *28S* ribosomal RNA (*28S* rRNA) were amplified by polymerase chain reaction (PCR), which was carried out in a reaction mix containing 1 μL of template DNA, 12 μL of Premix Taq™ (Takara, Otsu, Shiga, Japan), 1 μL of forward and reverse primers (10 mM), and 10 μL sterile distilled H_2O to a total volume of 25 μL.

COI, *16S*, and *28S* were amplified using the primers and protocols outlined by Hemery et al. (2012). PCR products were examined by 1.5% agarose gel electrophoresis and purified using EZ-10 Spin Column DNA Gel Extraction Kit (Sangon Biotech, Shanghai, China) prior to sequencing. The purified PCR products were sequenced in both directions using an ABI PRISM 3730 (Applied Biosystems, Thermo Fisher Scientific, Massachusetts, U.S.A.) automated DNA sequencer, using the same primer sets as for PCR amplification.

Sequence data was visualised and edited by the Seqman software (DNAS-TAR, Inc., Madison, Wisconsin, USA). Manual checks ensured the accuracy of the sequences. These sequences were checked against the nucleotide NCBI database through BLAST searches (https://blast.ncbi.nlm.nih.gov/doc/blast-help/references.html#references) to ensure that the sequences were uncontaminated. New sequences were deposited on GenBank (Table 2).

Two sequence datasets were analyzed. The first dataset included all existing *COI* barcoding sequences of *Endoxocrinus* and was used to perform species identification. The second dataset was used to determine the systematic status of new species of *Endoxocrinus*, *COI*, *16S* and *28S* concatenated sequences of seven *Endoxocrinus* taxa and an outgroup of *Panglaocrinus* (Table 2). For the protein-coding gene *COI*, alignment was performed with MEGA v.6 (Tamura et al. 2013) based on codon positions. The *16S* and *28S* sequences were instead aligned with default parameters using MAFFT v. 5 (Katoh et al. 2005), with G-INS-i strategy. Alignments were then trimmed using Gblocks 0.91 (Castresana 2000; Talavera and Castresana 2007) under default conditions. Kimura-2 parameter (K2P) genetic distances for *Endoxocrinus* were calculated using MEGA v. 6.

Phylogenetic trees were inferred using maximum likelihood (ML) and Bayesian inference (BI) analysis of tandem sequences. The most suitable partitioning scheme and replacement model were selected by PartitionFinder v. 2.1.1 (Lanfear et al. 2017) (*16S*, TrN+I+G; *COI*-1st codon, HKY+I+G; *COI*-2nd codon, SYM+I+G; *COI*-3rd codon, GTR+G; *28S*, TPM2+F). ML analysis was performed using the IQ-TREE web server (Trifinopoulos et al. 2016), with best-fit partitioning scheme and models, selected with PartitionFinder v. 2.1.1. Branch support was assessed by 5000 ultra-fast bootstrap replications (Minh et al. 2013). BI analyses were performed with MrBayes 3.1 (Ronquist and Huelsenbeck 2003) using the partitioning model, the same used for IQ-TREE. A Markov chain Monte Carlo (MCMC) was run for 5,000,000 generations, sampling every 500 generations to allow sufficient time for convergence. The first 25% of the sampled trees were discarded as burn-in. The remaining trees were used to estimate the consensus tree with 50% majority rule and Bayesian posterior probability (PP). At the end of the run, the mean standard deviation of the split frequency was reduced to 0.01. The effective sample size (ESS) values for all sampling parameters were checked by Tracer v. 1.7 (Rambaut et al. 2018) to ensure that convergence was achieved.

Table 2. List of sequences produced or retrieved from NCBI used in the barcoding and phylogenetic analysis of extant isocrinids.

Taxon	COI	16S	28S	Reference
E. (*Diplocrinus*) *kexuei* sp. nov. (holotype)	OR077296	OR082608	PQ770959	Present paper
E. (*Diplocrinus*) *kexuei* sp. nov. (paratype)	OR077297	PQ770958	PQ770960	Present paper
E. (*Diplocrinus*) *wyvillethomsoni*	OR237781	OR233480	OR233473	Améziane et al. 2023
E. (*Endoxocrinus*) *parrae*	OR237782	GU327874	OR233474	Améziane et al. 2023
E. (*Diplocrinus*) *alternicirrus alternicirrus*	KC626541	KC626633	KC626821	Hemery et al. (2013)
E. (*Diplocrinus*) *alternicirrus sibogae*	KC626542	KC626634	KC626822	Hemery et al. (2013)
Panglaocrinus isseliformis	OR237780	OR233479	OR233472	Améziane et al. 2023
Proisocrinus ruberrimus	GU327842	GU327878	GU327949	Rouse et al. (2013)

Results and discussion

Systematics

Order Isocrinida Sieverts-Doreck, 1952
Family Balanocrinidae Roux, 1981
Subfamily Diplocrininae Roux, 1981
Genus *Endoxocrinus* A.H. Clark, 1908

Subgenus *Diplocrinus* Döderlein, 1912

Type species. *Pentacrinus maclearanus* Thomson, 1872.

***Endoxocrinus* (*Diplocrinus*) *kexuei* sp. nov.**
https://zoobank.org/7D41C791-0061-49C5-8CA1-9AA942E76F27
Figs 1−9

Material examined. *Holotype* • MBM287584, collected from one rotten piece of wood in the cold seep area of the Taixinan Basin, South China Sea, at the station FX-Dive 125 (22°02.58'N, 118°46.83'E), depth 833.7 m, hard substrate. *Paratype* • MBM287585 (one specimen), collection data same as the holotype.

Diagnosis. Arm number 20−22; arms smooth, up to 14 cm long; lateral flanges present on all proximal brachials; IB_{r1+2} synostosis very flat with synostosial stereom predominating; axial canal rectangular; stalk shorter than arms, 6.5 cm long; internodals per mature noditaxis 5−8; stalk stellate to pentagonal cross-section; proximalmost diameter of stalk 5 mm; less than five (down to 2) cirri per nodal; proximal cirri directed upward; cirrus sockets large and round; 30 robust cirrals per cirrus; cirri rudimentary until 3th nodal; cryptosymplexies without marked symmorphy and with facets mainly covered by synostosial stereom axial canal usually incompletely filled with stereom needlelike network and preserving an irregular secondary lumen

Etymology. The species name is derived from the oceanographic vessel "Kexue" of the Institute of Oceanology, Chinese Academy of Sciences, which made a significant contribution to the biological research in the South China Sea.

Description. *Morphological description of the holotype.* Specimen MBM287584 (Figs 1−6). Colour (Fig. 1a, b) pale yellow-pink in fresh samples, and white after alcohol immersion. Several arms and all cirri broken.

Arms 22, surface smooth, whole arm length 8−17cm; two or three divisions per ray, two of these rays have three divisions, rays closely aligned (Fig. 2a); all brachitaxes of two ossicles, united by non-muscular joints (synostosis). On all free arms, the first two brachials are connected by a synostosis muscular articulations present on the remaining branchials. IB_{r1} rectangular with distal lateral margins weakly everted. IB_{r2} pentagonal with lateral margin somewhat thickened and crenulated. IIB_{r1+2} and $IIIB_{r1+2}$ with lateral flanges. IIB_{r1} and $IIIB_{r1}$ with exterior lateral margin longer than interior. Proximal brachials (up tp B_{r6}) approximately square, with varying degrees of crenulate on lateral margin, the edge regular, flat and close to straight, giving a very angular appearance to the brachials.

The non-functional ligamentary articulations IB_{r1+2}, IIB_{r1+2} and $IIIB_{r1+2}$, are clearly identified as synostosis. The synostosis of IB_{r1+2} very flat with synostosial

Figure 1. *Endoxocrinus* (*Diplocrinus*) *kexuei* sp. nov., holotype (MBM287584) **a** photograph of the entire organism taken directly after collection presenting the original colour **b** overall photo after preservation in alcohol. Scale bars: 1 cm.

stereom predominating and rectangular axial canal (Fig. 5a, b). However, at IIB_{r1+2} and $IIIB_{r1+2}$ (Fig. 5c–f), while synostosial stereom predominats and, syzygial stereom forms rudimentary crenularium near the aboral edge of the facet; the syzygial stereom remains very irregular on the lateral edges.

On the free arms, non-muscular junctions are present only in B_{r1+2}, whose general morphological features are similar to the secundibrachial or tertibrachials synostosis, with synostosial stereom forming a rudimentary crenularium on the aboral margin of the articular facet (Fig. 6a, b). The rest of the brachial articulations are typical isocrinid synarthries (Fig. 6c, d).

Basals form quadrilateral projections, protruding and separated from each other (W/L = 1.4–1.6). Radials hexagonal or pentagon, laterally adjacent (W/L = 2.4–2.8).

First pinnule (P_1) on B_{r2} (Fig. 3a), with 9–11 pinnulars, approximately 8.1 mm long; second pinnular longest, up to 1.4 mm, penultimate segment slender, twice as long as wide. P_2 to P_4 short and wide; proximal segments relatively long, middle segments longest, and distal segments abruptly narrowed and shortened. P_{10} to P_{15} longest and slender, about 13.5–16.5 mm long, with 17–19 pinnulars; proximal segment wider, middle segments longer than wide (L/W = 1.4–1.6); distal pinnulars with small spines on dorsal edges. Pinnules gradually becoming shorter towards the distal of the arm. P_{20} to P_{29} composed of 6–15 segments, pinnulars longer than wide (L/W = 1.6–2.0), except the first pinnular.

Stout stalk about 7.8 cm long and counts 39 whole columnals, distal nodal slightly broken proximal stalk gradually turning from star-shaped to pentagonal in cross-section, 5 mm in diameter proximally and 4.3 mm distally, the longest noditaxis is the seventh (6.92 mm) with eight nodals, proximal nodals are
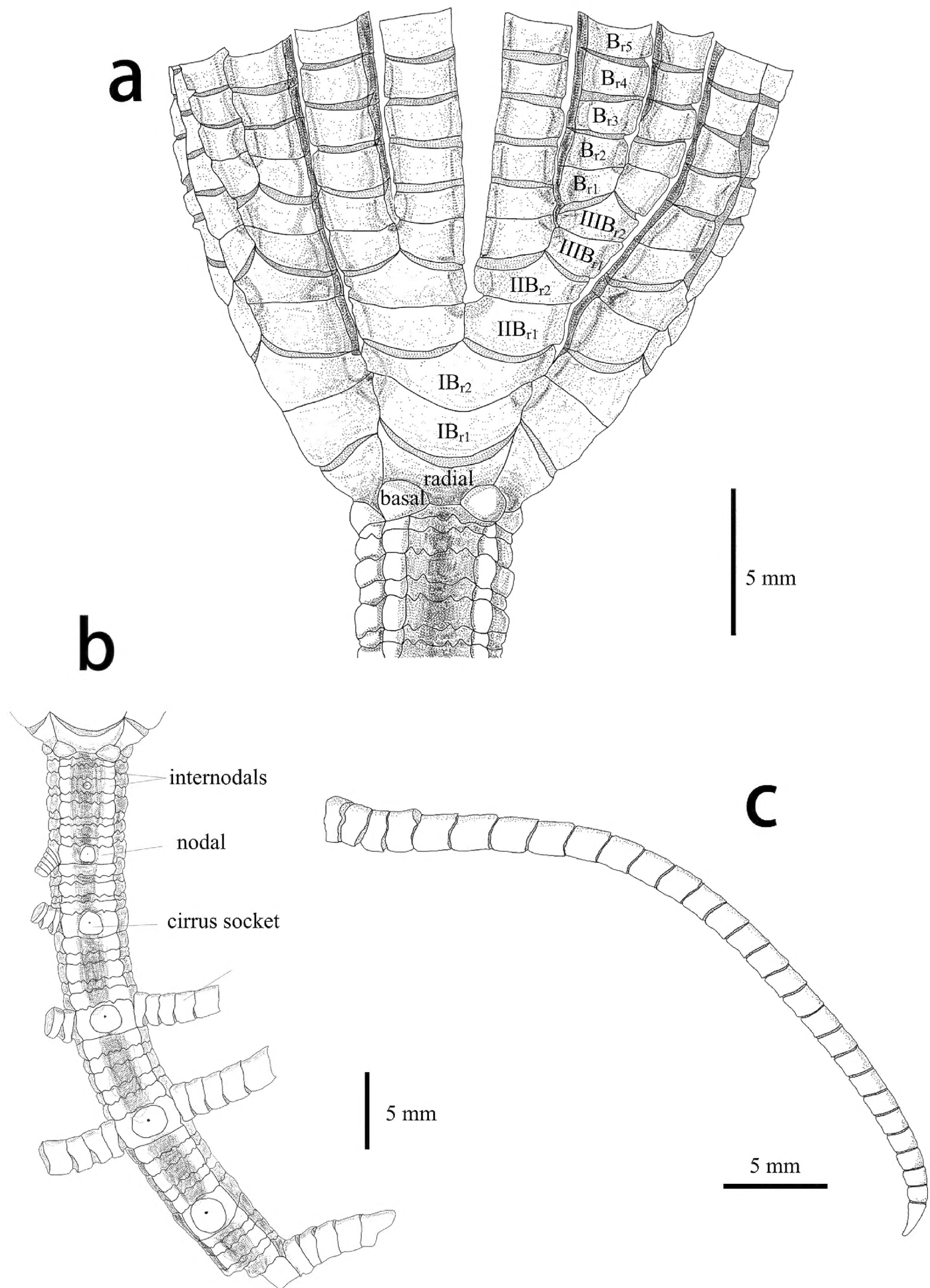
Figure 2. *Endoxocrinus* (*Diplocrinus*) *kexuei* sp. nov., holotype (MBM287584) **a** proximal stalk and base of crown **b** entire stalk **c** detail of complete cirrus. Scale bars: 5 mm.

1.2 mm in height and distal ones being 2.1 mm tall in this noditaxis; less than 5 cirri on each nodal, usually two or three, four on the 6th nodal and two on the 7th nodal. Proximal cirri directed upward, forming an acute angle with the proximal stalk; rudimentary cirri on the first to third nodal. The number of interrnodal per noditaxis is 5 (Fig. 2b). Between two nodals, the internodal exactly in the middle is slightly higher than the others. Cirri remaining rudimentary, usually before the 3th nodal. Fully developed cirrus slender with 30 cirrals, 6.3−8.5 cm long (Fig. 2c) (others incomplete or missing); cirrus sockets large and round, occupying approximately the entire height of nodal (Fig. 2b). The first 3 segments are relatively short. c_1−c_4 with W/L = 1.7−2.3; c_5 to c_9 longest, longest cirral with W/L = 0.8−1; subsequent cirrals gradually shorter, c_{13}−c_{15} with W/L = 1.0−1.1; terminal claw quite small, slightly longer than the penultimate segment, no opposing spine; distalmost three cirri curved downward for fixation.

Nodal and infranodal united by cryptosymplexy. The cryptosymplexy (Fig. 4a) is pentalobate and flat, with synostosial stereom occupying most of it and syzygial stereom restricted to its outer margin. The round axial canal (Fig. 4b) is partially filled with a relatively long spicule network separated from the perilumen and preserving an irregular secondary lumen. Petaloid zones (Fig. 4c) pear-shaped, interpetaloid zone is dominated by syzygial stereom and without axial groove. Symplexies present between internodals (Fig. 4d), each petaloid zone having 6−8 crenulae and open lanceolate areola and interpetaloid zone (Fig. 4e) is dominated by labyrinthic stereom.

Morphological description of the paratype. Specimen MBM287585 (Figs 7−9) incomplete, part of the stalk and all cirri are missing (Fig. 6b). Paratype is similar to the holotype, yet smaller. Differences are listed below.

20 smooth arms, up to 7−8 cm long. Two brachials per brachitaxes and two divisions per ray. IB$_{r1+2ax}$ and IIB$_{r1+2ax}$ (Fig. 8a). Proximal branchials with lateral edges less waved than in the holotype. Branchial surface smooth. IB$_{r1+2}$, IIB$_{r1+2}$ and IIIB$_{r1+2}$, have small lateral flanges.

Basals rhombic, prominent and obviously apart from each other, W/L = 1.1−1.5. Radials hexagonal or pentagon, W/L = 1.9−2.3.

P1 on B$_{r2}$ (Fig. 8b), with 8−9 pinnulars. Oral pinnule short; proximal pinnulars thick and wide, distal pinnulars become slender and longer. Middle pinnule longest, with 11−13 pinnulars, 13.0 mm long. At the end of arms, pinnule shorter or absent.

The remaining stalk length is about 1.7 cm, proximal column cross-section stellate to pentagonal.

Proximal infranodal columnal facet (Fig. 9a) with slight symmorphy in inner part, pear-shaped petaloid zones, and axial canal completely filled with dense thin stereom network without secondary lumen (Fig. 9c). Cryptosymplexies (Fig. 9b) relatively flat without marked symmorphy and with facets mainly covered by synostosial stereom. Outer margin zone and interpetaloid zone with syzygial stereom predominating. Axial canal (Fig. 9d) markedly pentagonal and partially filled with a relatively long spicule network separated from the perilumen and preserving an irregular secondary lumen.

Quantitative morphological characters are reported in Table 1.

Distribution. Only known from the cold seep in the Taixinan Basin, South China Sea, at a depth of 833.7 m.
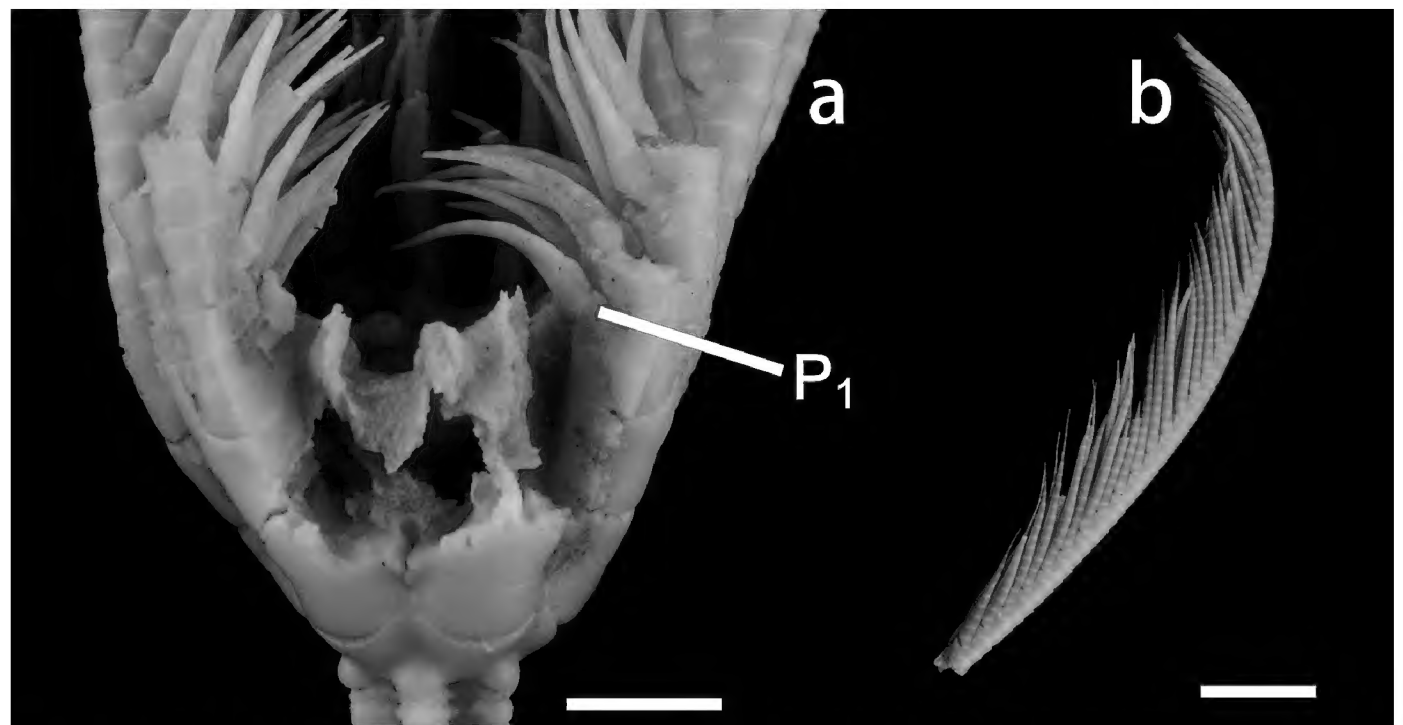
Figure 3. *Endoxocrinus* (*Diplocrinus*) *kexuei* sp. nov., holotype (MBM287584) **a** general view of crown **b** general view of pinnulars. P_1: first pinnule. Scale bars: 5 mm (**a**); 1 cm (**b**).

Remarks. The genus *Endoxocrinus* now contains four extant species. According to David et al. (2006), the new species resembles mostly *E.* (*Diplocrinus*) *alternicirrus* in terms of arm division series, shape of the cross-section of stalk, and the number of internodal per mature noditaxis (Table 3). In *E.* (*Diplocrinus*) *alternicirrus*, the arms are up to 64 in number and 10–12 cm in length, while in *E.* (*Diplocrinus*) *kexuei* sp. nov., the arms are only 20–22 in number and are shorter (8–14 cm). The number of arms is variable among *Endoxocrinus* species (Table 3). The arm number is usually considered as an adaptive trait that often depends on depth, food supply and hydrodynamics (Roux 1987; David et al. 2006). In *E.* (*Diplocrinus*) *kexuei* sp. nov., the proximal cirri are directed upward and cirri are rudimentary until the 3th nodal, differing from *E.* (*Diplocrinus*) *alternicirrus*, in which the proximal cirri are oriented downward and cirri are rudimentary until 5th nodal. These characteristics are similar to *E.* (*Diplocrinus*) *wyvillethomsoni*, in which the proximal cirri are oriented upward and the rudimentary cirri are present to the 3rd nodal.

Cryptosymplexies exhibit traits that are more relevant at the species level. In *E.* (*Diplocrinus*) *kexuei* sp. nov., the cryptosymplexies present no marked symmorphy with facets mainly covered by synostosial stereom, while in *E.* (*Diplocrinus*) *alternicirrus*, the interpetaloid zone of cryptosymplexies with syzygial stereom predominating but with strong symmorphy in inner portion. In *E.* (*Diplocrinus*) *wyvillethomsoni* and *E.* (*Endoxocrinus*) *parrae*, cryptosymplexies are flat or with slight symmorphy with syzygial stereom predominating on interpetaloid zones. In *E.* (*Diplocrinus*) *maclearanus*, the cryptosymplexies with undulating symmorphic surface, synostosial stereom predominating on interpetaloid zones. The difference in the characteristics of stalk cryptosymplexy supports our classification at the species level rather than at the subspecies level, in accordance with Roux (1977) and David et al. (2006). The axial canal structures show distinct differences among *Endoxocrinus* species. In *E.* (*Diplocrinus*) *kexuei* sp. nov., the axial canals are incompletely filled with long spicules, separated from the perilumen and preserve an irregular secondary lumen, while in *E.* (*Diplocrinus*) *alternicirrus*, the axial canals are completely filled with a dense mesh of long thin spicules without secondary lumen (Fig. 4f) (Roux 1977, David et al. 2006). In *E.* (*Diplocrinus*) *maclearanus*, *E.* (*Endoxocrinus*) *parrae* and

E. (*Diplocrinus*) *wyvillethomsoni*, the axial canal is filled with short thick spicules, large meshed stereom, and irregular network, respectively. In *E.* (*Diplocrinus*) *maclearanus* and *E.* (*Endoxocrinus*) *parrae*, the secondary lumen is small or absent. *Endoxocrinus* (*Endoxocrinus*) *parrae* has a small to large secondary lumen.

Key to the genus *Endoxocrinus*

1 $IIIB_r$ and following series of three ossicles, developed exteriorly................
.................***Endoxocrinus* (*Endoxocrinus*) *parrae* (Gervais in Guérin, 1835)**
– $IIIB_r$ and following series, when present, of two ossicles only **2**
2 Internodes long, usually of 20–56 columnals (mode 32)...........................
.... ***Endoxocrinus* (*Diplocrinus*) *wyvillethomsoni* (Thomson, 1872)**
– Internodes fewer columnals, usually of 5–14 ....**3**
3 Cirri usually 5 per nodal ....
........................***Endoxocrinus* (*Diplocrinus*) *maclearanus* (Thomson, 1878)**
– Less than 5 cirri per nodal **4**
4 Preserving an irregular secondary lumen ....
....***Endoxocrinus* (*Diplocrinus*) *kexuei* sp. nov.**
– No secondary lumen ....
............................***Endoxocrinus* (*Diplocrinus*) *alternicirrus* (Carpenter, 182)**

Figure 4. SEM views of stalk articulations in *Endoxocrinus* (*Diplocrinus*) *kexuei* sp. nov., holotype (MBM287584)(**a–e**); *E.* (*Diplocrinus*) *alternicirrus* (David et al. 2006, fig 20b) (**f**); cryptosymplexy (**a–c, f**) symplexy (**d–e**). **a** Distal nodal facet **b** and **f** close up on stereom within axial canal **c** petaloid and interpetaloid zone of cryptosymplexy **d** symplexy of an internodal's facet **e** petaloid and interpetaloid zone of the symplexy. Scale bars: 1 mm (**a, c–e**); 100 μm (**b, f**).

Table 3. Comparison of the diagnoses of the *Endoxocrinus* species, summarized from David et al. (2006).

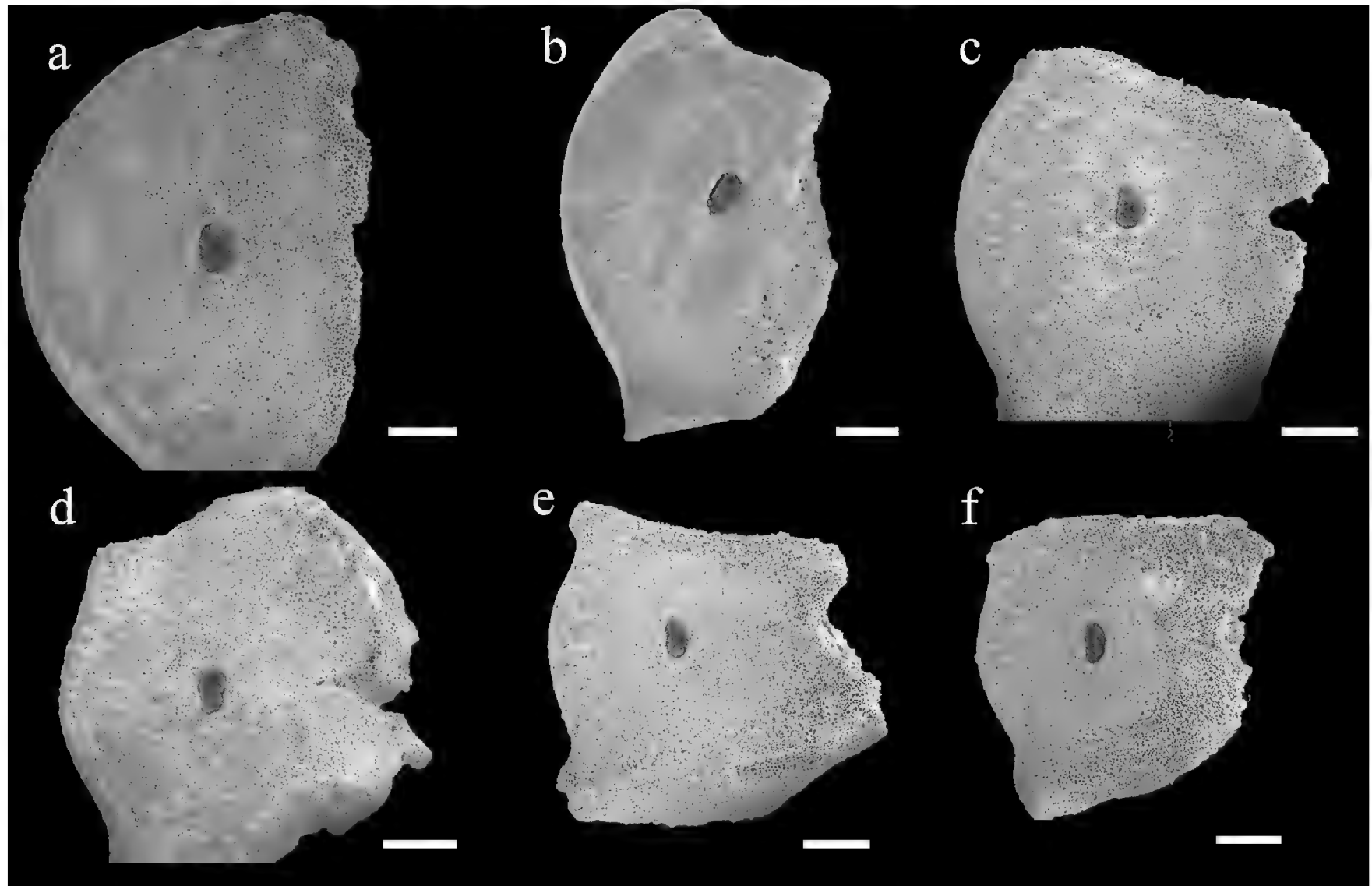| E. (*Diplocrinus*) *kexuei* sp. nov.	E. (*Diplocrinus*) *alternicirrus*	E. (*Diplocrinus*) *maclearanus*	E. (*Diplocrinus*) *wyvillethomsoni*	E. (*Endoxocrinus*) *parrae*
arms 20−22	arms up to 64	arms 14−30	arms 10−21	arms 23−58
arms smooth	arms smooth	arms smooth	arms smooth	arms smooth to serrated
arms 8−14 cm long	arms up to 15.3 mm long	arms up to 10 cm long	arms up to 10.5 cm long (mean 7 cm)	–
IB_{r1+2} synostosis very flat with synostosial stereom predominating	IB_{r1+2} synostosis relatively flat with synostosial stereom predominating, small syzygial crenulation near aboral edge of facet	proximal synostoses at B_{r1+2} relatively flat with syzygial stereom irregularly developed	non-muscular articulation B_{r1+2} intermediate between synostosis and syzygy, showing a general symmorphy, tending to a true synostosis distally and to a syzygy between primibrachials	–
stalk axial canal rectangular	stalk axial canal rectangular	stalk axial lumen rectangular	axial canal lumen bilobate	–
stalk length about 6.5 cm long	stalk length variable up to 14 cm	stalk <9 cm long (mean 3.8 cm)	stalk length strongly variable, 3.5−22.5 cm	–
internodals per mature noditaxis 5−8	internodals per mature noditaxis 4−10 usually 5−6	internodals per mature noditaxis usually 6−14	internodals per mature noditaxis 20−56 (mode 32)	internodals per mature noditaxis usually 6−14 (mode in local populations 8−12)
stalk stellate to pentagonal cross-section	stalk stellate to pentagonal cross-section	stalk pentalobate to pentagonal cross-section	middle and distal stalk pentagonal to circular in cross-section	stalk in adult pentalobate to pentagonal in cross-section
prox stalk diameter 5 mm	prox stalk diameter 4−6 mm up to 7.9 mm	prox stalk diameter up to 5.1 mm	prox diameter of stalk up to 4.2 mm (mean 2.9 cm)	prox diameter of stalk usually 4−5 mm
less than 5 cirri per nodal	less than 5 cirri per nodal	cirri usually 5 per nodal	always 5 robust cirri per nodal	usually 5 cirri per nodal
Proximal cirri directed upward	proximal cirri oriented downward	cirri oriented upward	proximal cirri oriented upward	–
cirrus sockets large and round	cirri socket nearly circular	–	–	–
The first 3 segments are relatively short, c5 to c9 longest, subsequent cirrals gradually shorter	cirrals long	–	–	–
up to 30 robust cirrals per cirrus	up to 35 cirrals per cirrus (usually 28−30)	–	–	with up to 44 cirrals per cirrus (usually >30)
cirri rudimentary until 3th nodal	cirri rudimentary until 5th nodal	–	rudimentary cirri present to 3rd nodal	–
cryptosymplexies without marked symmorphy and with facets mainly covered by synostosial stereom	interpetaloid zone of cryptosymplexies with syzygial stereom predominating but with strong symmorphy in inner portion	cryptosymplexies with undulating symmorphic surface, synostosial stereom predominating on interpetaloid zones	cryptosymplexies flat or with slight general symmorphy with syzygial stereom predominating on interpetaloid zones and on a regular outer border of the facet	cryptosymplexies flat or with a slight symmorphy of inner interpetaloid zone, with syzygial stereom predominating in interpetaloid zones
axial canal usually incompletely filled with stereom needlelike network, separated from perilumen	axial canal with long thin spicules, distinct from perilumen	axial canal filled with short thick spicules clearly separated from perilumen	axial canal filled up by large meshed stereom not clearly separated from perilumen	axial canal filled up by an irregular and variable network not clearly separated from perilumen
preserving an irregular secondary lumen	no secondary lumen	secondary lumen small or absent	secondary lumen small or absent	a small to large secondary lumen
Western Pacific	Western Pacific	Eastern Brazil, Bahamian	South European Atlantic Shelf, Eastern Caribbean	Gulf of Mexico and Caribbean Sea
833.7 m	600−2000 m	200−300 m	1000−3000 m	150−2000 m

Figure 5. *Endoxocrinus* (*Diplocrinus*) *kexuei* sp. nov., holotype (MBM287584) **a** distal facet of IBr1 **b** proximal facet of IBr2 **c** distal facet of IIBr1 **d** proximal facet of IIBr2 **e** distal facet of IIIBr1 **f** proximal facet of IIIBr2. Scale bars: 600 μm.
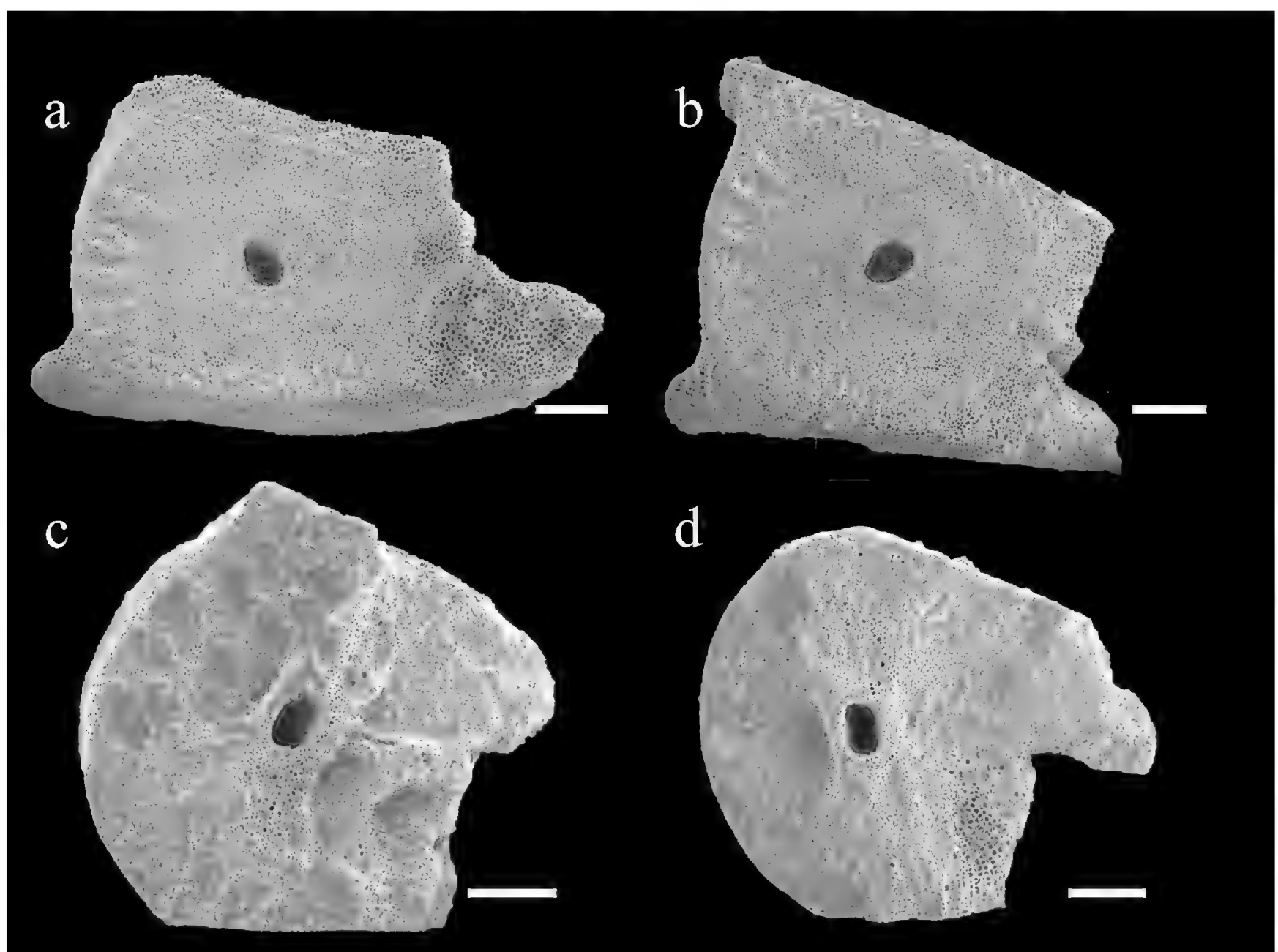

Figure 6. *Endoxocrinus* (*Diplocrinus*) *kexuei* sp. nov., holotype (MBM287584) **a** distal facet of br1 **b** proximal facet of br2 **c** distal facet of br5 **d** proximal facet of br6. Scale bars: 400 μm.

Figure 7. *Endoxocrinus* (*Diplocrinus*) *kexuei* sp. nov., paratype (MBM287585) **a** photograph of the entire organism taken directly after collection presenting the original colour **b** overall photo after preservation in alcohol. Scale bars: 1 cm.
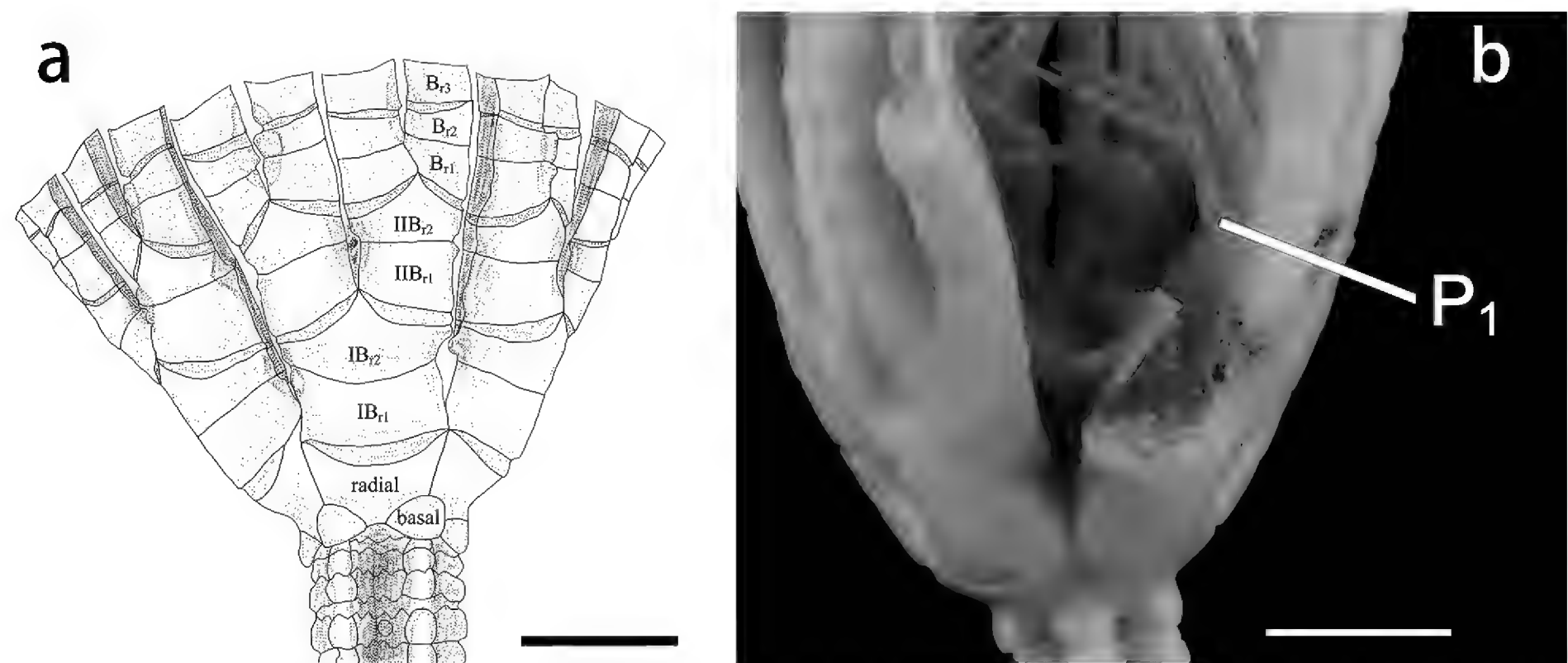
Figure 8. *Endoxocrinus* (*Diplocrinus*) *kexuei* sp. nov., paratype (MBM287585) **a** proximal stalk and base of crown **b** general view of crown, P_1, first pinnule. Scale bars: 5 mm.

Barcoding, phylogenetic relationships, and taxonomic implication

The interspecific genetic distance (K2P) within the genus *Endoxocrinus* was calculated based on the *COI* gene. The interspecific distances within *Endoxocrinus* ranged from 2.1% to 8.5%. The genetic distance within the new species is 0.5%. *Endoxocrinus* (*Diplocrinus*) *kexuei* sp. nov. showed the shortest genetic distance with *E.* (*Diplocrinus*) *alternicirrus* (2.1–2.5%) and the greatest distance
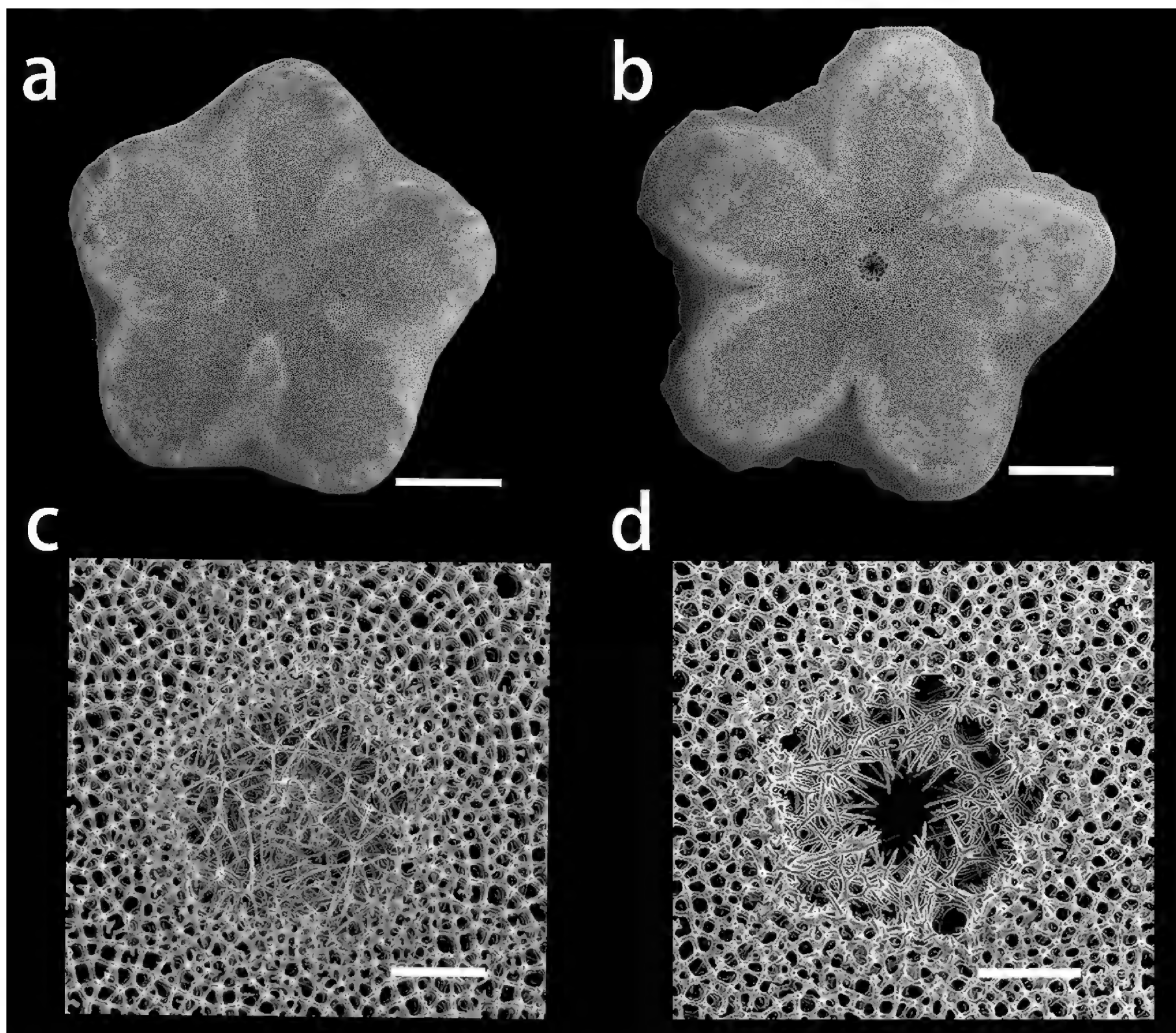
Figure 9. SEM views of cryptosymplexies in *Endoxocrinus* (*Diplocrinus*) *kexuei* sp. nov., paratype (MBM287585) **a–c** and **b–d** are from two different articulations **b–d** being more proximal **a** proximal infranodal facet **b** distal nodal facet **c** and **d** close-ups on the axial canal. Scale bars: 1 mm (**a, b**); 100 μm (**c, d**).

with *E.* (*Diplocrinus*) *wyvillethomsoni* (7.9%) (Table 4). The phylogenetic tree of extant *Endoxocrinus* derived from BI and ML analyses showed consistent results (Fig. 10). *Endoxocrinus* (*Diplocrinus*) *kexuei* sp. nov. is nested within *Endoxocrinus* and is sister clade to *E.* (*Diplocrinus*) *alternicirrus*. Both the genetic distance and phylogenetic relationship are consistent with the classification based on morphological evidence. *E.* (*Diplocrinus*) *kexuei* sp. nov. is similar to its congener *E.* (*Diplocrinus*) *alternicirrus*, with the same division series, cross-section of stalk, and the same number of internodals per mature noditaxis.

Conclusion

Based on morphology and phylogenetic analysis, one *Endoxocrinus* species is recognized and described as new to science in this study: *Endoxocrinus* (*Diplocrinus*) *kexuei* sp. nov. The new species is similar to *E.* (*Diplocrinus*) *alternicirrus* in external morphology, but differs by showing cryptosymplexies without marked symmorphy, and an axial canal usually incompletely filled with a lattice
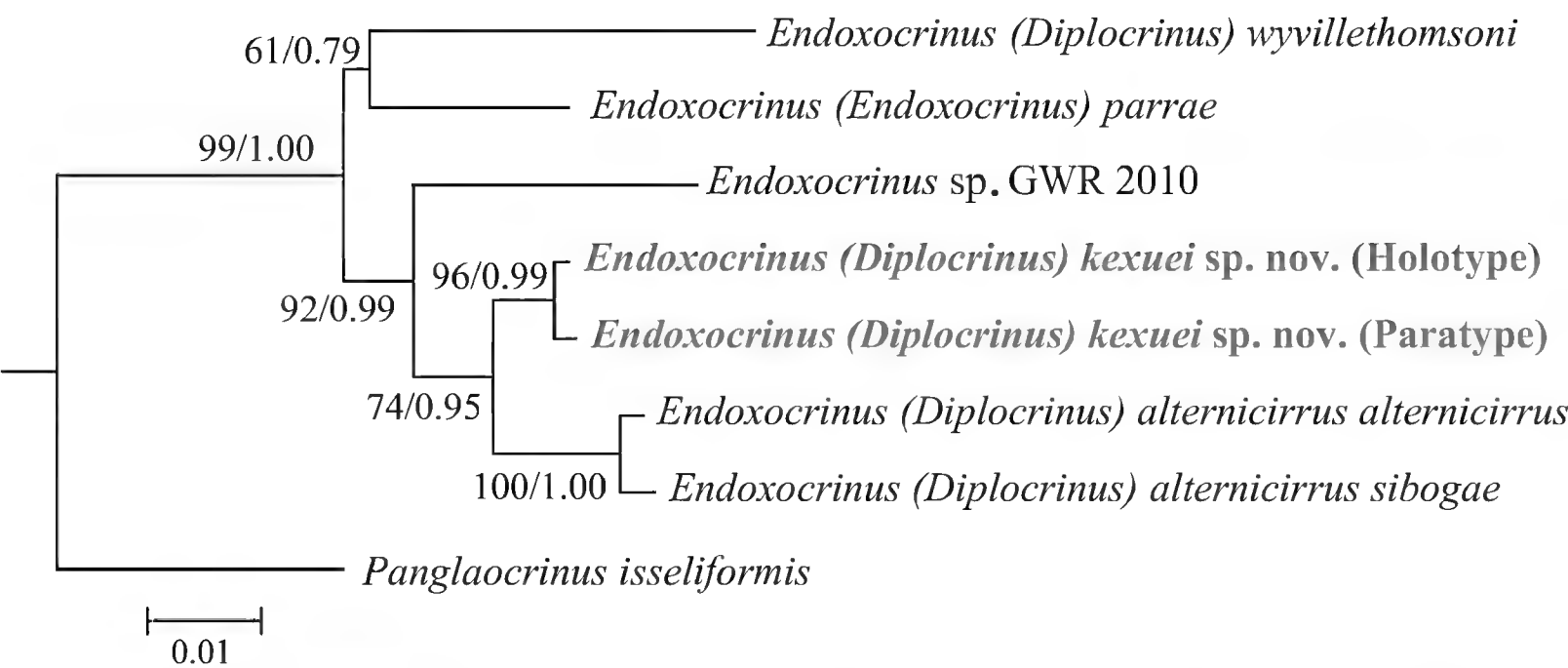
Figure 10. Maximum-likelihood (ML) tree of *Endoxocrinus* using combined sequences of *COI* (619 bp), *16S* (328 bp) and *28S* (736 bp). As the topologies of ML or BI are congruent, the ML tree was used to represent the phylogeny. The number at each node represents bootstrap values (BP) (left) and Bayesian posterior probability (BPP) (right). The new species is highlighted in red.

Table 4. The genetic distance of *COI* gene (K2P) within *Endoxocrinus* species.

	1	2	3	4	5	6	7
1 *E. (Diplocrinus) kexuei* sp. nov. (holotype)							
2 *E. (Diplocrinus) kexuei* sp. nov. (paratype)	0.005						
3 *E. (Diplocrinus) wyvillethomsoni*	0.079	0.081					
4 *E. (Endoxocrinus) parrae*	0.060	0.062	0.078				
5 *E. (Diplocrinus) alternicirrus alternicirrus*	0.025	0.030	0.085	0.069			
6 *E. (Diplocrinus) alternicirrus sibogae*	0.021	0.026	0.081	0.069	0.006		
7 *Endoxocrinus* sp. GWR-2010	0.042	0.047	0.074	0.061	0.051	0.047	

needlelike network, preserving an irregular secondary lumen. The phylogenetic analysis provided support for the establishment of the new species. The genetic distances between the new species and *E.* (*Diplocrinus*) *alternicirrus* are the smallest. *Endoxocrinus* (*Diplocrinus*) *kexuei* sp. nov. is the first extant stalked crinoid discovered in a cold seep area in the South China Sea.

Acknowledgements

Additional information

Conflict of interest

The authors have declared that no competing interests exist.

Ethical statement

No ethical statement was reported.

Author contributions

Data curation, Sun Shao'e, Mei Zijie, and Sha Zhongli; formal analysis, Sha Zhongli; funding acquisition, Sha Zhongli; writing – original draft, Sun Shao'e, Mei Zijie; writing – review and editing, Sun Shao'e, Mei Zijie, and Sha Zhongli. All authors have read and agreed to the published version of the manuscript.

Author ORCIDs

Shao'e Sun ⓘ https://orcid.org/0009-0003-5774-6209
Zijie Mei ⓘ https://orcid.org/0009-0002-6818-0565
Zhongli Sha ⓘ https://orcid.org/0000-0002-2192-3758

Data availability

In accordance with FAIR principles, the *COI*, *16S* and *28S* sequences in this study (Suppl. material 1) can be found in the Supplemental Materials and openly available in GenBank.

References

Améziane N, Roux M (1997) Biodiversity and historical biogeography of stalked crinoids (Echinodermata) in the deep sea. Biodiversity & Conservation 6: 1557–1570. https://doi.org/10.1023/A:1018370620870

Améziane N, Eléaume M, Roux M (2023) Classification of Isocrinida (Echinodermata: Crinoidea) with the description of a new extant genus and species from the western Pacific. Zoological Journal of the Linnean Society 200(4): 994–1012. https://doi.org/10.1093/zoolinnean/zlad101

Berndt C, Crutchley G, Klaucke I, et al. (2014) Geological controls on the gas hydrate system of Formosa Ridge, South China Sea. OCEANS 2014 – TAIPEI, Taipei, Taiwan. https://doi.org/10.1109/OCEANS-TAIPEI.2014.6964481

Carpenter PH (1882) The stalked crinoids of the Caribbean Sea. In: Reports on the results of dredging under the supervision of Alexander Agassiz, in the Gulf of Mexico (1877–78), and in the Caribbean Sea (1878–79), by the U.S. Coast Survey Steamer "Blake", Bulletin of the Museum of Comparative Zoology 10 (4): 165–181.

Castresana J (2000) Selection of conserved blocks from multiple alignments for their use in phylogenetic analysis. Molecular biology and evolution 17(4): 540–552. https://doi.org/10.1093/oxfordjournals.molbev.a026334

Clark AH (1908) Two new crinoid genera. Proceedings of the Biological Society of Washington 21: 149–152.

David J (1998) Adaptation morphologique, croissance et production bioclastique chez les crinoïdes pédonculés actuels et fossiles (Pentacrines et Millericrinina). Application paléoécologiques aux gisements du Jurassique supérieur des Charentes et du Nord-Est du Bassin de Paris. Thèse, Université de Reims, Sciences de la Terre, 2 vol., 551 pp.

David J, Roux M, Messing CG, Améziane N (2006) Revision of the pentacrinid stalked crinoids of the genus *Endoxocrinus* (Echinodermata, Crinoidea), with a study of environmental control of characters and its consequences for taxonomy. Zootaxa 1156: 1–50. https://doi.org/10.11646/zootaxa.1156.1.1

Döderlein L (1907) Die gestielten Crinoiden der Siboga-Expedition: Siboga expeditie. Uitkomsten op zoologish, botanish, oceanographish Oost-Indie (1899–1900), Leiden 42a: 1–54.

Döderlein L (1912) Die gestielten Crinoiden der deutschen Tiefsee-Expedition. Wissenschaftliche Ergebnisse der deutsche Tiefsee-Expedition auf dem Dampfer "Valvidia" (1898–1899), Jena G. Fischer 1902–40. https://doi.org/10.5962/bhl.title.12010

Feng D, Qiu JW, Hu Y, Peckmann J, Guan H, Tong H, Chen C, Chen J, Gong S, Li N, Chen D (2018) Cold seep systems in the South China Sea: An overview. Journal of Asian Earth Sciences 168: 3–16. https://doi.org/10.1016/j.jseaes.2018.09.021

Forel M-B, Charbonnier S, Gale L, Tribovillard N, Martinez-Soares P, Bergue CT, Felix M. Gradstein, Gaillard C (2024) A new chemosynthetic community (ostracods, foraminifers, echinoderms) from Late Jurassic hydrocarbon seeps, south-eastern France Basin. Geobios 84: 1–24. https://doi.org/10.1016/j.geobios.2023.12.006

Gervais FLP (1835) Encrine. In: Guérin MF-E., Dictionnaire pittoresque d'histoire naturelle et des phénomènes de la nature. Paris, Au Bureau de Souscription. 3: 49–50. [pl. 147]

Hemery LG, Eléaume M, Roussel V, Améziane N, Gallut C, Steinke D, Cruaud C, Couloux A, Wilson NG (2012) Comprehensive sampling reveals circumpolarity and sympatry in seven mitochondrial lineages of the Southern Ocean crinoid species *Promachocrinus kerguelensis* (Echinodermata). Molecular Ecology 21: 2502–2518. https://doi.org/10.1111/j.1365-294X.2012.05512.x

Hemery L, Michel R, Améziane N, Eléaume M (2013) High-resolution crinoid phyletic inter-relationships derived from molecular data. Cahiers de Biologie Marine 54: 511–523. https://doi.org/10.21411/CBM.A.1FE819C4

Hunter AW, Larson NL, Landman NH, Oji T (2016) Lakotacrinus brezinai n. gen. n. sp., a new stalked crinoid from cold methane seeps in the Upper Cretaceous (Campanian) Pierre Shale, South Dakota, United States. Journal of Paleontology 90: 506–524. https://doi.org/10.1017/jpa.2016.21

Kato M (2019) Crinoids lived around the Cretaceous seeps: the second example from cold-seep deposit in the Yezo Group in Hokkaido, Japan. Zoosymposia 15: 88–97. https://doi.org/10.11646/zoosymposia.15.1.10

Kato M, Oji T, Shirai K (2017) Paleoecology of echinoderms in cold seep environments revealed by isotope analysis in the late cretaceous western interior seaway. Palaios 32: 218–230. https://doi.org/10.2110/palo.2016.079

Katoh K, Kuma K, Toh H, Miyata T (2005) MAFFT version 5: improvement in accuracy of multiple sequence alignment. Nucleic Acids Research 33: 511–518. https://doi.org/10.1093/nar/gki198

Lanfear R, Frandsen PB, Wright AM, Senfeld T, Calcott B (2017) PartitionFinder 2: New methods for selecting partitioned models of evolution for molecular and morphological phylogenetic analyses. Molecular Biology and Evolution 34: 772–773. https://doi.org/10.1093/molbev/msw260

Minh BQ, Nguyen MAT, von Haeseler A (2013) Ultrafast Approximation for Phylogenetic Bootstrap. Molecular Biology and Evolution 30: 1188–1195. https://doi.org/10.1093/molbev/mst024

Rambaut A, Drummond AJ, Xie D, Baele G, Suchard MA (2018) Posterior Summarization in Bayesian Phylogenetics Using Tracer 1.7. Systematic Biology 67: 901–904. https://doi.org/10.1093/sysbio/syy032

Ronquist F, Huelsenbeck JP (2003) MrBayes 3: Bayesian phylogenetic inference under mixed models. Bioinformatics 19: 1572–1574. https://doi.org/10.1093/bioinformatics/btg180

Rouse GW, Jermiin LS, Wilson NG, Eeckhaut I, Lanterbecq D, Oji T, Young CM, Browning T, Cisternas P, Helgen LE, Stuckey M, Messing CG (2013) Fixed, free, and fixed: The fickle phylogeny of extant Crinoidea (Echinodermata) and their Permian–Triassic origin. Molecular Phylogenetics and Evolution 66: 161–181. https://doi.org/10.1016/j.ympev.2012.09.018

Roux M (1977) The stalk-joints of recent Isocrinidae (Crinoidea). Bulletin of the British Museum (Natural History). Zoology 32: 45–64.

Roux M (1981) Echinodermes: Crinoïdes Isocrinidae. In: Forest J (Ed.) Résultats des Campagnes MUSORTOM I – Philippines (18–28 mars 1976). Mémoires O.R.S.T.O.M., Paris, 91, 477–543.

Roux M (1987) Evolutionary ecology and biogeography of recent stalked crinoids as a model for the fossil record. In: Jangoux M, Lawrence JM (Ed.) Echinoderm Studies. A.A. Balkema, Rotterdam, 2, 1–53.

Roux M, Messing CG, Améziane N (2002) Artificial keys to the genera of living stalked crinoids (echinodermata). Bulletin of marine science 70: 33.

Roux M, Améziane N, Eléaume M (2009) The genus *Teliocrinus* (Crinoidea, Echinodermata): a key taxon among pentacrinid stalked crinoids. Zoological Journal of the Linnean Society 155: 22–39. https://doi.org/10.1111/j.1096-3642.2008.00392.x

Sieverts-Doreck H (1952) Isocrinida. In: Moore RC, Lalicker CG, Fischer AG (Eds) Invertebrate Fossils. New York: McGraw-Hill BookCompany, 766.

Talavera G, Castresana J (2007) Improvement of phylogenies after removing divergent and ambiguously aligned blocks from protein sequence alignments. Systematic Biology 56: 564–577. https://doi.org/10.1080/10635150701472164

Tamura K, Stecher G, Peterson D, Filipski A, Kumar S (2013) MEGA6: Molecular Evolutionary Genetics Analysis Version 6.0. Molecular Biology and Evolution 30: 2725–2729. https://doi.org/10.1093/molbev/mst197

Thomson W (1872). 2. On the Crinoids of the "Porcupine" Deep-Sea Dredging Expedition. Proceedings of the Royal Society of Edinburgh 7: 764–773. https://doi.org/10.1017/S037016460004308X

Thomson CW (1878) The Voyage of the "Challenger". The Atlantic. A preliminary account of the general results of the exploring voyage of H.M.S. "Challenger" during the year 1873 and the early part of the year 1876, Volume 2 viii+340 pp. (Macmillan & Co.). https://doi.org/10.5962/bhl.title.79255

Trifinopoulos J, Nguyen L-T, von Haeseler A, Minh BQ (2016) W-IQ-TREE: a fast online phylogenetic tool for maximum likelihood analysis. Nucleic Acids Research 44: W232–W235. https://doi.org/10.1093/nar/gkw256

Zhang W, Liang JQ, Liang QY et al. (2021) Gas Hydrate Accumulation and Occurrence Associated with Cold Seep Systems in the Northern South China Sea: An Overview. Geofluids, 5571150 https://doi.org/10.1155/2021/5571150

Supplementary material 1

Six sequence datasets from two specimens

Authors: Shao'e Sun, Zijie Mei, Zhongli Sha

Data type: txt

Explanation note: Sequence information needed to construct phylogenetic trees.

Link: https://doi.org/10.3897/zookeys.1241.128991.suppl1